Macromolecules

pubs.acs.org/Macromolecules
Article

Effect of Stiffness on the Dynamics of Entangled Nanofiber Networks at Low Concentrations

Ahmad Reza Motezakker,* Andrés Córdoba, Tomas Rosén, Fredrik Lundell, and L. Daniel Söderberg*

Cite This: *Macromolecules* 2023, 56, 9595−9603
Read Online

ABSTRACT: Biopolymer network dynamics play a significant role in both biological and materials science. This study focuses on the dynamics of cellulose nanofibers as a model system given their relevance to biology and nanotechnology applications. Using large-scale coarse-grained simulations with a lattice Boltzmann fluid coupling, we investigated the reptation behavior of individual nanofibers within entangled networks. Our analysis yields essential insights, proposing a scaling law for rotational diffusion, quantifying effective tube diameter, and revealing release mechanisms during reptation, spanning from rigid to semiflexible nanofibers. Additionally, we examine the onset of entanglement in relation to the nanofiber flexibility within the network. Microrheology analysis is conducted to assess macroscopic viscoelastic behavior. Importantly, our results align closely with previous experiments, validating the proposed scaling laws, effective tube diameters, and onset of entanglement. The findings provide an improved fundamental understanding of biopolymer network dynamics and guide the design of processes for advanced biobased materials.

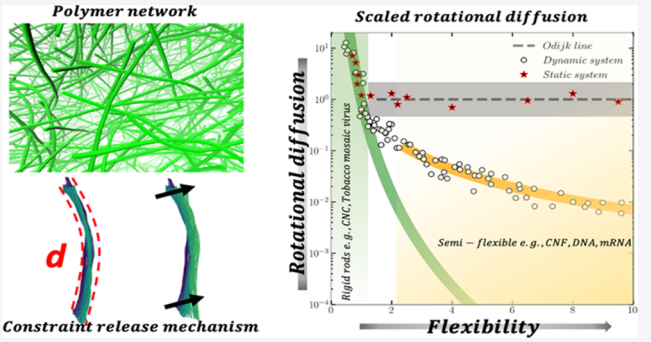

INTRODUCTION

Biopolymer networks, both in natural and synthetic forms, play a critical role in numerous scientific and technological advancements.[1] These networks serve as the architectural elements in various vital systems, providing structural integrity and functional properties.[2] Examples include the cytoskeletal components of eukaryote cells, such as actin filaments and microtubules, as well as collagen nanofibrils in connective tissues, chitin nanofibrils in arthropod exoskeletons, fibroin nanofibrils in silk, and cellulose nanofibers (CNFs) in plant cell walls.[3−6] The exceptional properties exhibited by biopolymer networks have sparked considerable interest in utilizing them as the basis for developing advanced, sustainable materials. In recent years, cellulose nanofibers have emerged as a prominent class of biopolymers, attracting significant attention due to their unique properties. CNFs, categorized as semiflexible biopolymers, exhibit remarkable characteristics, such as low density, high strength, high stiffness, and chemically adjustable surfaces.[7,8] These attributes make CNFs highly promising as nanoscale building blocks for creating high-performance materials with potential applications in diverse fields.[9−13]

The dynamics of semiflexible nanofibers within entangled media is important for developing advanced biobased materials. Understanding these dynamics expands our knowledge of fundamental cellular processes like cell division, cell motility, and intracellular transport and paves the way for the design and optimization of nanotechnologies, including nanorobots and nanosensors.[14] In condensed matter physics, the reptation model, initially proposed by De Gennes[15,16] and later extended by Edwards[17] and Doi,[18,19] serves as a theoretical framework for comprehending the dynamics of highly concentrated (entangled) dispersions of polymers. This model describes the motion of a polymer chain within an imaginary tube defined by the transient network of entangled neighboring chains. The chain moves in a snake-like manner inside the tube, constrained by the surrounding matrix. The reptation model successfully captures the behavior of entangled polymer chains, with long time scales exhibiting liquid-like viscosity and short time scales resembling rubber-like behavior. The idea of a chain moving within a tube, hindered from lateral deformations due to topological restrictions, has been experimentally validated and has significantly contributed to our understanding of entangled polymer solutions.[20,21] While experimental techniques, such as neutron and light scattering[22−25] and fluorescence autocorrelation spectroscopy,[26,27] have been employed to probe the dynamics of entangled polymers in bulk, obtaining detailed information about the temporal and spatial dynamics of

Received: July 31, 2023
Revised: October 18, 2023
Accepted: November 9, 2023
Published: November 20, 2023

https://doi.org/10.1021/acs.macromol.3c01526
Macromolecules 2023, 56, 9595−9603

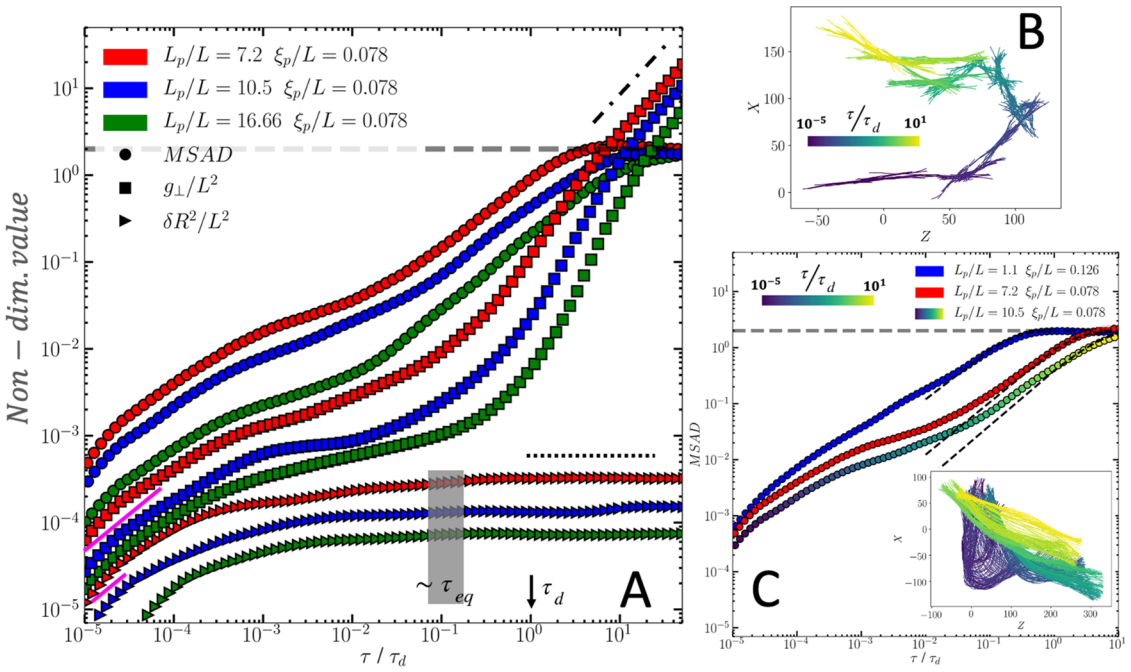

Figure 1. Dynamics of fibers as a function of stiffness. (A) Projected length fluctuations δR^2, orthogonal mean squared displacement of the centered monomer of fibers $g_\perp$, and mean squared angular displacement of the normalized end-to-end vector MSAD for three L_p/L at a fixed mesh size. The solid magenta lines show the $t^{3/4}$ behavior of $g_\perp$ and δR^2 in the initial stage of the simulations, the dotted line represents the saturated stage of δR^2, and the dash-dotted line shows the linear diffusive stage of the system. (B) Projection of the 3D motion of a nanofiber onto the x−z plane. (C) Comparison of MSAD of entangled and dilute cases. The color bar in (B, C) corresponds to time within the temporal framework.

individual polymer chains, as well as the role of heterogeneity and molecular individualism, remains a significant challenge.

However, observing polymer motion in entangled environments, including the small-scale fluctuations that occur on the order of milliseconds and involve several monomer units, remains a challenging task. To address these challenges, numerical simulations have emerged as powerful tools for studying the dynamics of entangled polymer chains in crowded environments. Simulations offer a unique opportunity to investigate the behavior of individual nanofibers, unravel constraint release mechanisms, and explore their influence on larger-scale properties. By delving into the intricacies of reptation behavior and employing advanced simulation methods, researchers can gain deeper insights into the behavior of individual polymer chains, providing a more comprehensive understanding of biopolymer dynamics and paving the way for the design and optimization of high-performance materials.

Building upon these scientific foundations, the present work focuses on employing simulations and comparative analysis to enhance our understanding of the reptation behavior of cellulose nanofibers (CNFs) and the related implications for the processing of advanced materials. The simulation-based approach allows for a detailed examination of individual CNFs within entangled media, shedding light on the constraints they experience and the mechanisms governing their motion. Furthermore, the comparative analysis with experimental data, including previously published results in microrheology, serves to validate the simulation findings and establish their significance in the field. By elucidating the intricacies of CNF dynamics in entangled environments, this work contributes to the current understanding of biopolymer networks and offers valuable insights for the design and development of advanced biobased materials.

RESULTS AND DISCUSSION

Per definition, the persistence length quantifies the bending stiffness of a polymer by relating it to the thermal (Brownian) forcing, i.e., $L_p = \kappa/k_BT$, where κ is the bending stiffness, k_B is the Boltzmann constant, and T is the absolute temperature. Thus, a low persistence length indicates worm-like dynamics and a high persistence length indicates rod-like behavior.

The conventional polymer reptation model assumes that the time scale for a chain moving through a tube is shorter than the time scale for reconformation of the tube, neglecting the effects of entanglement caused by the particle shape and stiffness. It was proposed by Odijk[28] that even slight flexibility increases the rotational diffusion of fibers, $1/D_r \propto L^2L_p$, which contradicts Doi's argument[19] that rotational diffusion is independent of fiber stiffness, $1/D_r \propto L^7/\xi_p^4$, where ξ_p is the mean distance between the fibers. Odijk's prediction $\left(D_r \approx \frac{k_BT}{\mu L_p L^2}\right)$ is supported by a thorough experimental investigation into the Brownian motion of carbon nanotubes in a porous static agarose gel network[29] with controlled confinement. However, given the results presented in this work, there are two conceptual perspectives to consider. First, in a realistic system of entangled semiflexible to rigid fibers, all fibers experience confinement while undergoing thermal motion in a dynamic matrix instead of a static one, where rotation is a significant component. Second, a priori understanding of the agarose concentration at which confinement becomes significant is missing. Although Kremer verified the reptation motion in entangled systems using simulations,[30] Skolnick and Fixman contended that reptation is not the predominant mechanism in such systems.[31,32]

The main goal of our computational experiments is to quantify the effects of entanglement and link the dynamics of

https://doi.org/10.1021/acs.macromol.3c01526
Macromolecules 2023, 56, 9595−9603

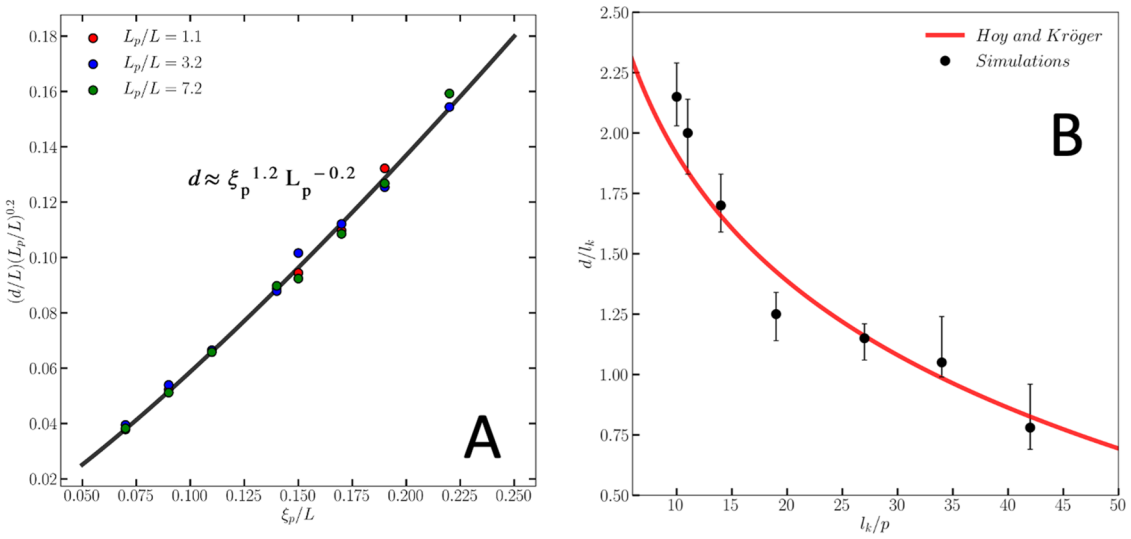

Figure 2. Effective tube diameter analysis. (A) The correlation between the predicted effective tube diameter d, ξ_p, and L_p of the system as $d \approx \xi_p^{1.2} L_p^{-0.2}$. (B) Comparison between our simulation results to the results from Hoy and Kröger.[38]

semiflexible to rigid polymers/fibers to the macroscopic rheological behavior of biopolymer-based materials. This has been performed using coarse-grained molecular dynamics (MD) simulations based on the ESPResSo software package,[33] which allows the coupling to hydrodynamic interactions using the lattice Boltzmann method (LBM). The simulated nanofibers were constructed using a bead−spring model, in which repulsion is the only interaction between the fibers. Each simulated case represents a dispersion of fibers having a length L, width b, and persistence length L_p. At a given number of fibers per unit volume, ν, the mean distance between the fibers can be estimated by the geometrical mesh size $\xi_p = \sqrt{3/(\upsilon L)}$. The details of the modeling can be found in the Methods Section. Values for fiber Young's modulus (between 4.5 and 18.4 GPa) and fiber dimensions were selected based on previously reported values for high-charge TEMPO-oxidized CNF.[34] More details on simulations and the parameters are provided in Supporting Information (SI), S1−S3.

We have chosen to work with three key nondimensional observables to characterize the nanofiber dynamics and system relaxation:

- The mean-squared displacement of the end-to-end distance (projected length), δR^2 (t), provides insights into the bending dynamics of individual fibers in the network.
- The rotational diffusion is characterized using the mean-squared angular displacement of the normalized end-to-end vector, MSAD.
- The normal mean-squared displacement of the midpoints of the fibers, $g_\perp$ (t), provides an understanding of the effect of confinement.

The additional details of the observables are provided in Supporting Information (SI), S4.

In Figure 1A, we can see the evolution of these parameters for three distinct cases. In a dilute dispersion, where the nanofibers diffuse freely, the projected length fluctuations typically increase with time as $t^{3/4}$, until reaching a plateau value $L^4/45L_p$ at nanofiber equilibration time τ_{eq}. More crowded systems exhibit similar behavior but with a transitional regime before the plateau caused by confinement induced by surrounding fibers, correlating to the onset of entanglement, and are thus referred to as the entanglement time τ_e. At the end of the transitional regime, when the bending dynamics of the nanofibers δR^2 have equilibrated, confinement is no longer sensed and the system has reached the equilibrium time. This time scale appears to be more sensitive to the concentration of the system than to the bending stiffness, where it is shown that the time required for internal relaxation grows as the crowdedness of the system increases, i.e., smaller ξ_p/L (see Figure S3). The results show that τ_{eq} is significantly shorter than it takes for a nanofiber to diffuse its entire length or erase its history τ_d. This contradicts the fundamental assumption of reptation theory, which suggests that a polymer fully traverses its length within the tube before significant reconformation of the tube.

Furthermore, this provides insights regarding τ_d, which is the longest relaxation time of the system and proportional to the inverse of rotational diffusion. If we consider $u(t)$ as the unit vector of the end-to-end distance of a nanofiber, we can write the unit vector correlation function as

$$\langle u(t+\tau)\cdot u(t)\rangle \sim \langle \cos\theta\rangle \sim \exp(-2D_r t)$$

where θ is the angular displacement and $2D_r$ is proportional to decay time, which is $1/\tau_r$. Thus, we can write MSAD as

$$\langle (u(t+\tau) - u(t))^2\rangle = 2(1 - \exp(-2D_r t))$$

At short times, when both $D_r t$ and θ are small, we can consider $\cos\theta \sim 1 - \theta^2/2$, resulting in MSAD $\sim 4D_r t$. At longer times, $t \to \infty$, the initial and final direction of the unit vector will be uncorrelated, $\langle u(t+\tau)\cdot u(t)\rangle = 0$, and MSAD will consequently saturate to 2, as can be seen in Figure 1A. The same MSAD behavior can be observed regarding the diffusion of free fibers in a dilute dispersion (Figure 1B). As expected, confinement in the crowded systems introduces a separation between the short- and long-term behavior of MSAD. In the long-term, both MSAD and trajectory analysis indicate that fibers rotate like rigid rods (Figure 1C). Therefore, we can estimate D_r by fitting the long-term MSAD data to $2(1 - \exp(-2D_r t))$, as predicted for rigid rods.[18]

By studying $g_\perp$, it is possible to estimate the direct effects of confinement, and similar to δR^2, as shown by the solid magenta

https://doi.org/10.1021/acs.macromol.3c01526
Macromolecules 2023, 56, 9595−9603

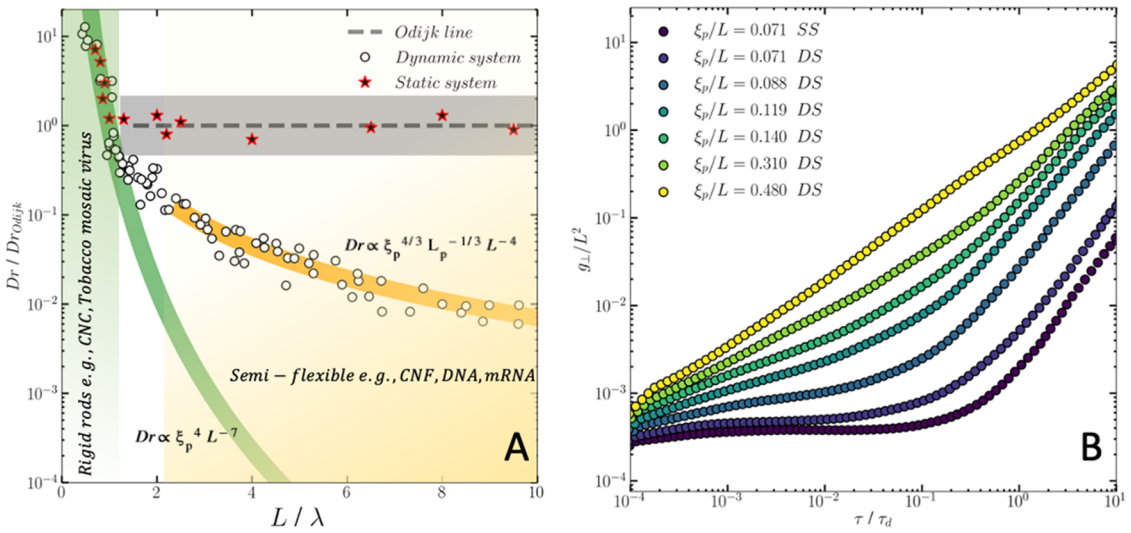

Figure 3. Diffusivity of nanofibers. (A) Normalized rotational diffusivity of nanofibers in a dynamic system with various L_p/L and ξ_p/L values versus the length normalized with the deflection length. The dashed gray line represents Odijk's prediction, and the green line represents Doi's prediction. The gray shading represents Fakhri's experimental results.[29] (B) The gradual decrease in the concentration of nanofiber dispersion for L_p/L = 3.2, illustrating the transition from a robust tubing effect to one that is weak or not observable in $g_\perp/L^2$.

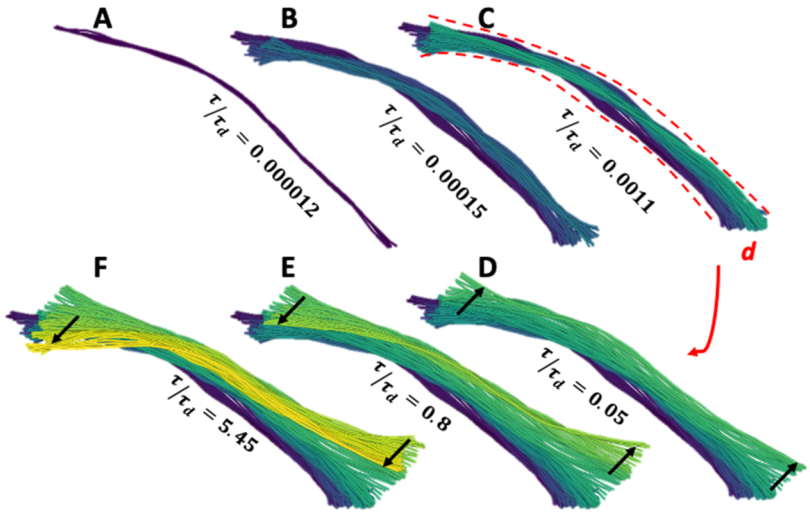

Figure 4. Time-dependent behavior of a single nanofiber in the entangled system of L_p/L = 7.2 and ξ_p/L = 0.098. The color map shows relative timing, and black arrows represent instantaneous motion of the nanofibers. (A) The first stage of the motion. (B) The nanofiber reptates along its length in the tube. (C) At this moment, the tube size and shape are distinguishable. (D) The nanofiber is liberated from the tube, and the constraint is released. (E) After being liberated, the nanofiber explores further and shows a turning move, coupling translation, and rotation. (F) The nanofiber continues to diffuse freely in space until it is trapped in a new tube.

line in Figure 1A, it increases as $t^{3/4}$ initially,[35] followed by a transition that seems to be related to the entanglement time, i.e., when the bending fluctuations of the fibers encounter confinement from their surroundings. The transition between these two states serves as a reference point for estimating the hypothetical tube diameter d (see Figure S4 in the SI). As shown in Figure 2A, our results indicate a relation between the tube diameter and the mesh size of the system as $d \approx \xi_p^{1.2} L_p^{-0.2}$, which is consistent with Rubinstein and Colby's works,[36,37] indicating that the tube diameter is always larger than the mesh size. In addition, the conflicting proposals for the scaling of polymer melts[39−42] have recently been addressed by Hoy and Kröger[38] by formulating an analytical expression for the reduced tube diameter, valid across the entire range of polymer stiffnesses. The evaluation of these parameters is based on a topological analysis of chain trajectories using the Z1 algorithm.[43] To compare our results with theirs, we have estimated the Kuhn length, l_k, and packing length, p, taking into account the flexibility of the chains and the number density of the networks, see Figure 2B. We observe similar trends to Hoy and Kröger for the tube diameter, but some discrepancies may arise from differences in the methods used to estimate these quantities.

After escaping initial confinement, $g_\perp$ indicates a super-diffusive behavior of the nanofibers, presumably traveling a complex route, i.e., a combined translational and rotational motion.[44,45] Finally, $g_\perp$ shows linear diffusion behavior upon reaching the longest relaxation time, τ_r.

To facilitate comparison, we present D_r in Figure 3A in the same manner as in Fakhri et al.[29] The vertical axis represents the ratio of D_r to Odijk's model prediction, $D_r \propto L^{-2} L_p^{-1}$, while the horizontal axis is given by

https://doi.org/10.1021/acs.macromol.3c01526
Macromolecules 2023, 56, 9595−9603

$$\mathcal{L} \approx L/\lambda = \sqrt[3]{(L/L_p)(L/\xi_p)^2}$$

which is the length normalized by the deflection length of the thermal undulation of the fibers. In principle, $\mathcal{L}$ is proportional to the inverse of the stiffness of the nanofibers. Given the obtained curves, we identify various ranges for $\mathcal{L}$. For $\mathcal{L} < 1$, it is evident that D_r agrees with Doi's prediction $D_r \propto \xi_p^4 L^{-7}$, suggesting that fibers act like rigid rods and that flexibility does not influence rotational diffusion. Within this limit, the largest possible orthogonal fluctuations of bending modes, L^3/L_p, are smaller than ξ^2, and Doi and Edwards' mechanism of reptation−rotation predicts the motion of the fibers. However, for $\mathcal{L} > 2.3$, flexibility does have a significant impact, where $D_r \propto \xi_p^{4/3} L_p^{-1/3} L^{-4}$, indicating that terminal relaxation occurs faster than Doi's prediction but slower than Odijk's prediction. The shaded region in Figure 3A represents simulations by Lang & Frey,[46] consistent with the latter. As a comparison to the results for dynamic systems, our calculated cases for fibers moving in static systems can be observed to lie within the gray-shaded area, thus conforming to Odijk's prediction and earlier published results.

In Figure 3B, we present the orthogonal fluctuation of fibers for various cases of ξ_p/L with $L_p/L = 3.2$. A closer look at the case of $\xi_p/L = 0.071$ (SS), i.e., in a static system, reveals that $g_\perp$ is relatively stable for a while, indicating that the fiber is confined inside the static tube until it exits, rotates, and enters a new tube, confirming the classic reptation theory and other simulations with static systems.[47,48] For the similar case g in a dynamic system, $\xi_p/L = 0.071$ (DS), there are similarities observed compared to the static case. Initially, $g_\perp$ remains constant, followed by an earlier increase. This suggests that in a real dynamic system, the semiflexible polymers undergo thermal motion (rotation and translation) that compromises the existence of a tube as defined in the conventional reptation theory, i.e., it is possible for a tube to reconform entirely before the trapped polymer reptates its length.

To further investigate the mechanisms involved, the dynamics of individual nanofibers was analyzed across a wide range of time scales to evaluate the constraint release mechanism. In Movie S2, this is exemplified by showing the dynamics of a single nanofiber for the case of $L_p/L = 7.2$ and $\xi_p/L = 0.098$ (an extra example is shown in Movie S3 for shorter nanofibers). The nanofiber dynamics is considered in multiple stages in Figure 4. The nanofiber is presented in an entangled environment in the first scene (A). As time passes, it becomes evident that the nanofiber reptates along the tube's length while remaining confined inside the tube (B). The nanofiber will continue to reptate in the next step (C), and at this point, the form (red dashed line) and diameter of the tube will be distinguishable. The fourth phase (D) is the point in time when the reconformation of the tube is significant, resulting in the release of the constraint. At this stage, the nanofiber breaks out from the original tube, as shown by the black arrow, and immediately moves to another region. In the subsequent stage (E), the nanofiber will continue to move freely while undergoing a turning motion. This motion highly couples the nanofiber's translation with its rotation. This phenomenon can explain the superdiffusive behavior of $g_\perp$ in the plots for entangled systems. The nanofiber continues its motion until it is confined in a new tube (F).

Several constraint release mechanisms, such as tube length fluctuations,[49,50] tube enlargement,[51,52] and convective constraint release,[20,53,54] have been proposed in the literature, but an understanding of the mechanism requires incorporating Marshal Fixman's notion of kinetic cages[55,56] and Bitsanis[57,58] proposed models. Fixman's theory proposes that the entropic cage surrounding a polymer is not static but instead undergoes fluctuations due to the thermal motions of the surrounding polymers. These fluctuations can lead to torque fluctuations, which can break the cage and increase the reorientation dynamics of the polymer. In essence, Fixman's theory suggests that polymer motion in crowded environments is governed by the interplay between entropic confinement and thermal fluctuations and that these dynamics can be understood by considering the geometry and fluctuations of the entropic cage surrounding the polymer. The Bitsanis model suggests that many-body effects contribute to the static properties much less than direct pair interactions; therefore, the local structure is mostly determined by independent binary interactions. The model suggests that the fluctuating entropic cage can create regions of high and low friction that affect the reptation dynamics of the polymer.

To gain a deeper understanding of the constraint release mechanism, we conducted two sets of simulations involving polymers with infinite persistent lengths (rigid rods). In the first set, a test rod is introduced into a static network of anisotropic rods, while in the second set, all of the rods in the network are allowed to move (Supporting, Movies S6 and S7, respectively). In the first case, the entropic cage surrounding the rigid rod polymer remained stable and static throughout the simulation. However, in the second case, the surrounding rod polymers were moving and continually bumping into the test rod, leading to fluctuations in the entropic cage surrounding the polymer. This is consistent with the Bitsanis model, which considers the dynamic nature of the entropic cage surrounding the polymer. The torque fluctuations observed in the dynamic case are a key mechanism underlying the dynamics of the entropic cage surrounding the polymer. As the surrounding polymers bump into the test rod, they create torques that can break the entropic cage, leading to faster reorientation dynamics of the polymer. Additionally, the second virial coefficient, which describes the strength of the excluded volume interactions between polymer chains, can play an important role in the dynamics of the entropic cage and the overall reptation motion of the polymer.

In the dynamic case, the second virial coefficient may influence the density and arrangement of the surrounding polymers, which, in turn, can affect the entropic cage surrounding the polymer and the dynamics of the reptation motion. In the literature, a gap exists in the current understanding of the constraint release mechanism, particularly regarding the consideration of semiflexibility. Previous investigations have largely overlooked the impact of semiflexible nanofibers, resulting in a limited understanding of the dynamics involved. This oversight is noteworthy because the semiflexibility of nanofibers dampens the effects of tube length fluctuations and tube enlargement. Our simulations, however, reveal a distinct behavior, where the constraint release mechanism exhibits a closer resemblance to the convective constraint release mechanism. In essence, the interplay between semiflexibility and the intricate dynamics of constraint release challenges conventional assumptions. The validity of the tube assumption is thus coupled to a clear separation of time scales between the particle concerned and its surroundings. As discussed by Lang & Frey,[46] the conditions for which

https://doi.org/10.1021/acs.macromol.3c01526
Macromolecules 2023, 56, 9595−9603

the tube assumption is valid have largely been ignored and are thus still up for discussion.

The analysis of Figure 3B provides insights into the onset condition of entanglement, focusing on the ratio of the polymer persistence length (stiffness) to the contour length. Notably, the concentration is carefully regulated until the tubing effect becomes discernible. To explore this phenomenon comprehensively, extensive investigations were conducted across a wide range of L_p/L values. The outcomes are presented in Figure 5, which depicts the relationship between

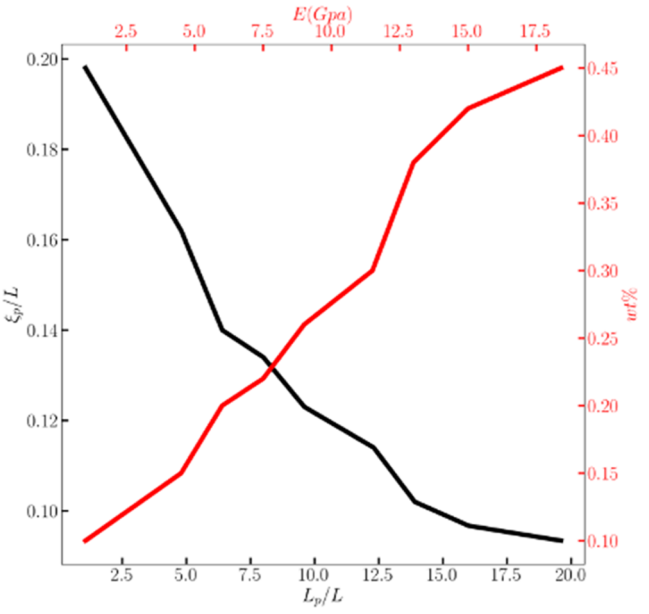

Figure 5. Relationship between the onset condition of tubing and fiber stiffness. The more flexible fibers exhibit tubing effects at lower network concentrations compared to those of more rigid fibers.

the onset condition of tubing and fiber stiffness. Intriguingly, the graph demonstrates that more flexible fibers exhibit tubing effects at lower network concentrations. This observation can be attributed to the larger orthogonal fluctuations exhibited by flexible fibers, leading to narrower, instantaneous pathways for adjacent fibers. Consequently, confinements with lower concentrations are formed. To enhance the clarity and comprehensibility of the analysis, the results are presented on a secondary axis in red color. Specifically, the concentration values are expressed in weight percentage (wt %), while Young's modulus of the fibers in the network is represented in GPa. Supporting, Movies S4 and S5 illustrate this phenomenon by showcasing the dynamics of two nanofiber networks with identical concentrations but differing in the flexibility of their constituent nanofibers. These movies serve as valuable visual tools, enabling a deeper understanding of how fiber flexibility influences the formation of confinements and the overall behavior of the system.

Up to this point, we have addressed the general mechanisms related to nanofiber dynamics and collective effects, including the development of novel scaling laws for rotational diffusion, estimation of the effective tube size, and identification of the onset of entanglements. However, these findings directly correlate with the observed behavior in the networked systems and have a direct impact on the processing of dispersion of high aspect ratio CNF into high-performance material concepts, where the balance between the susceptibility to induced fiber alignment (by e.g., flow or electrical fields) and the entanglement needed to maintain structural integrity during processing and assembly.[9]

By quantification of the viscoelastic properties, we can gain insights and effectively compare our results with previous experiments, thus enhancing the overall applicability of our findings. This was accomplished by applying the methodology for passive microrheology, where the sample's rheological characteristics are estimated by introducing spherical particles[59] (see SI, S1).

The results can be found in Figure 6A, where at low frequencies, $\omega < 3 \times 10^2$ rad/s, $G'(\omega)$ follows $a \sim \omega^2$ scaling, which is expected in the terminal zone of the storage modulus of a viscoelastic fluid. In the terminal zone, all of the mechanical stress stored in the viscoelastic fluid has relaxed. The terminal zone is also observed in Figure 6B in $G''(\omega)$, where the scaling is $\sim\omega$, which is a characteristic of the loss

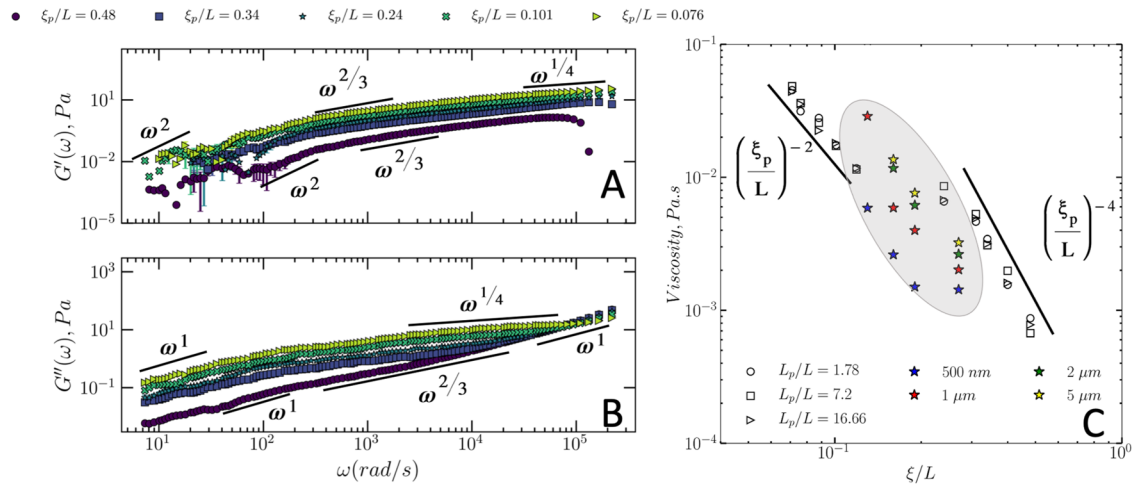

Figure 6. Microrheology of the dispersion and comparison to experiments. (A) Storage modulus, G', and (B) loss modulus, G'', measured with passive microrheology of CNF dispersion with L_p/L = 7.2 for different mesh sizes, ξ_p/L. (C) Zero shear viscosity of a cellulose dispersion with different mesh sizes estimated using the concept of passive microrheology. Colored markers represent estimates extracted from published experimental data.[63]

https://doi.org/10.1021/acs.macromol.3c01526
Macromolecules 2023, 56, 9595−9603

modulus of viscoelastic materials. This reflects the purely viscous response expected in the terminal zone. Both G' and G'' exhibit an $\sim\omega^{2/3}$ region at intermediate frequencies $3 \times 10^2 \lesssim \omega \lesssim 10^4$ rad/s, where the 2/3 scaling exponent has been observed for networks of actin filaments and is also typical of Zimm chains that interact hydrodynamically.[60] At higher frequencies, $\omega \gtrsim 10^4$ rad/s, G' appears to exhibit a transition toward a high-frequency plateau, which is more pronounced for networks with smaller mesh sizes. Also, at these frequencies, $G'' \sim \omega$, which indicates that for the networks with larger mesh sizes, the purely viscous response of the solvent dominates at high frequencies. For the dispersions with smaller mesh sizes, this scaling is only observed at $\omega \gtrsim 10^5$ rad/s, indicating that for the more concentrated networks, the viscoelastic response becomes dominated by the solvent at frequencies. It is also important to note that for large mesh sizes, $\xi_p/L \gtrsim 0.24$, G' is larger than G'' in the whole frequency range studied.

At around $\xi_p/L = 0.24$, a crossover between G' and G'' is observed. For smaller mesh sizes, G' becomes larger than G'' at higher frequencies, $\omega \gtrsim 7 \times 10^3$ rad/s. Thus, as a rule, an engineering rule of thumb for defining a transition threshold from flowing to nonflowing behavior of high-charge CNF systems, the mesh size $\xi_p/L \approx 0.24$ may be used, which corresponds to a concentration of 0.06 wt %, which is in agreement with published experimental results.[61,62] The nonflowing state at a lower mesh size is sometimes referred to as a volume-spanning arrested state, VAS.[63]

Figure 6C shows the zero shear viscosity of the cellulose dispersion with different mesh sizes, where the viscosity increases with a decreasing mesh size. We have compared our numerical findings with experimental results,[63] although determining zero shear viscosity using experimental techniques is challenging. As can be seen, some agreement can be seen when some assumptions are considered (SI, S5). At $\xi_p/L \approx 0.24$, there is a clear transition with respect to how the zero shear viscosity depends on the mesh size

$$\begin{cases} \xi_p/L < 0.24 \rightarrow \eta \sim (\xi_p/L)^{-2} \\ \xi_p/L > 0.24 \rightarrow \eta \sim (\xi_p/L)^{-4} \end{cases}$$

Note that the mesh size at which this change in the behavior of the viscosity occurs is the same mesh size at which the crossover between G' and G''starts to appear.

CONCLUSIONS

While the significance of understanding cellulose nanofiber (CNF) networks has been widely recognized for developing processing protocols in high-performance applications,[10,11] it is worth noting that the knowledge gained from these studies extends beyond CNFs. The principles and insights gained here can be applied to other engineering and biological systems involving semiflexible nanofibers, such as carbon nanotubes, metallic nanowires, or protein fibrils. Building upon this understanding, our study proposes a novel scaling law that describes the rotational diffusion of semiflexible nanofibers in entangled systems, highlighting the interplay between their rotational and translational motions. Additionally, we have evaluated the microrheology using our numerical experiments to complement our findings, demonstrating how simulations can serve as a powerful tool for coupling nanoscale dynamics to macroscopic and engineering properties. Expanding on this knowledge, future investigations could explore the dynamics, trapping, and hopping behavior of active and passive tracers within entangled biopolymer networks. This avenue of research has significant implications, particularly in areas such as the assembly of general nanofiber systems as well as, e.g., drug delivery concepts, where a thorough understanding of transport mechanisms and diffusion dynamics is crucial (see the SI, Movie S8).

ASSOCIATED CONTENT

Supporting Information

The Supporting Information is available free of charge at https://pubs.acs.org/doi/10.1021/acs.macromol.3c01526.

Ratio of bending stiffness from Young's modulus; tube diameter is estimated based on the transition point, and plotted observables for various cases (PDF)

Demonstration of nanofiber modeling for the special situation $L_p/L = 1.5$ and $\xi/L = 0.12$ (MP4)

Dynamics of a single nanofiber for the case of $L_p/L = 7.2$ and $\xi_p/L = 0.098$ breaking the cage (MP4)

Dynamics of a single fiber: breaking the cage (MP4)

Dynamics for the case of $L_p/L = 1.9$ and $\xi_p/L = 0.14$ (stiffness effect) (MP4)

Dynamics for the case of $L_p/L = 3.6$ and $\xi_p/L = 0.14$ (stiffness effect) (MP4)

Test rigid polymer in a fixed static network (MP4)

Test rigid polymer in a dynamic system (kinetic cages) (MP4)

Empty spaces between the nanofibers with time (MP4)

AUTHOR INFORMATION

Corresponding Authors

Ahmad Reza Motezakker − *Department of Engineering Mechanics, KTH Royal Institute of Technology, Stockholm SE-10044, Sweden; Wallenberg Wood Science Center, KTH Royal Institute of Technology, Stockholm SE-10044, Sweden*; Email: armot@kth.se

L. Daniel Söderberg − *Wallenberg Wood Science Center and Department of Fibre and Polymer Technology, KTH Royal Institute of Technology, Stockholm SE-10044, Sweden*; orcid.org/0000-0003-3737-0091; Email: dansod@kth.se

Authors

Andrés Córdoba − *Pritzker School of Molecular Engineering, University of Chicago, Chicago, Illinois 60637, United States*; orcid.org/0000-0001-8775-5251

Tomas Rosén − *Wallenberg Wood Science Center and Department of Fibre and Polymer Technology, KTH Royal Institute of Technology, Stockholm SE-10044, Sweden*; orcid.org/0000-0002-2346-7063

Fredrik Lundell − *Department of Engineering Mechanics, KTH Royal Institute of Technology, Stockholm SE-10044, Sweden*; orcid.org/0000-0002-2504-3969

Complete contact information is available at: https://pubs.acs.org/10.1021/acs.macromol.3c01526

Author Contributions

Conceptualization: A.R.M., L.D.S., T.R., and F.L. Methodology: A.R.M., L.D.S., and A.C. Investigation: A.R.M., L.D.S., and A.C. Funding acquisition: L.D.S. Project administration: L.D.S. Supervision: L.D.S., T.R., and F.L. Writing—original

https://doi.org/10.1021/acs.macromol.3c01526
Macromolecules 2023, 56, 9595−9603

draft: A.R.M., L.D.S., and A.C. Writing—review and editing: A.R.M., L.D.S., and A.C.

Notes

The authors declare no competing financial interest.

■ ACKNOWLEDGMENTS

The authors acknowledge the discussions and input to the work and the manuscript provided by Prof. Theo Odijk, Leiden University. They acknowledge financial support from Knut and Alice Wallenberg Foundation (KAW) through the Wallenberg Wood Science Center (A.R.M., F.L., and L.D.S.) and The Swedish Research Council grant 2018-06469 (T.R.).

■ REFERENCES

(1) Burla, F.; Mulla, Y.; Vos, B. E.; Aufderhorst-Roberts, A.; Koenderink, G. H. From Mechanical Resilience to Active Material Properties in Biopolymer Networks. *Nat. Rev. Phys.* **2019**, *1* (4), 249−263.

(2) Wegst, U. G. K.; Bai, H.; Saiz, E.; Tomsia, A. P.; Ritchie, R. O. Bioinspired Structural Materials. *Nat. Mater.* **2015**, *14* (1), 23−36.

(3) Gardel, M. L.; Shin, J. H.; MacKintosh, F. C.; Mahadevan, L.; Matsudaira, P.; Weitz, D. A. Elastic Behavior of Cross-Linked and Bundled Actin Networks. *Science* **2004**, *304* (5675), 1301−1305.

(4) Gitai, Z. The New Bacterial Cell Biology: Moving Parts and Subcellular Architecture. *Cell* **2005**, *120* (5), 577−586.

(5) Jansen, K. A.; Licup, A. J.; Sharma, A.; Rens, R.; MacKintosh, F. C.; Koenderink, G. H. The Role of Network Architecture in Collagen Mechanics. *Biophys. J.* **2018**, *114* (11), 2665−2678.

(6) Ling, S.; Kaplan, D. L.; Buehler, M. J. Nanofibrils in Nature and Materials Engineering. *Nat. Rev. Mater.* **2018**, *3* (4), No. 18016.

(7) Klemm, D.; Kramer, F.; Moritz, S.; Lindström, T.; Ankerfors, M.; Gray, D.; Dorris, A. Nanocelluloses: A New Family of Nature-based Materials. *Angew. Chem., Int. Ed.* **2011**, *50* (24), 5438−5466.

(8) Li, T.; Chen, C.; Brozena, A. H.; Zhu, J. Y.; Xu, L.; Driemeier, C.; Dai, J.; Rojas, O. J.; Isogai, A.; Wågberg, L.; Hu, L. Developing Fibrillated Cellulose as a Sustainable Technological Material. *Nature* **2021**, *590* (7844), 47−56.

(9) Rosén, T.; Hsiao, B. S.; Söderberg, L. D. Elucidating the Opportunities and Challenges for Nanocellulose Spinning. *Adv. Mater.* **2021**, *33* (28), No. 2001238.

(10) Håkansson, K. M. O.; Fall, A. B.; Lundell, F.; Yu, S.; Krywka, C.; Roth, S. V.; Santoro, G.; Kvick, M.; Wittberg, L. P.; Wågberg, L.; Söderberg, L. D. Hydrodynamic Alignment and Assembly of Nanofibrils Resulting in Strong Cellulose Filaments. *Nat. Commun.* **2014**, *5* (1), No. 4018.

(11) Mittal, N.; Ansari, F.; Gowda V, K.; Brouzet, C.; Chen, P.; Larsson, P. T.; Roth, S. V.; Lundell, F.; Wagberg, L.; Kotov, N. A.; et al. Multiscale Control of Nanocellulose Assembly: Transferring Remarkable Nanoscale Fibril Mechanics to Macroscale Fibers. *ACS Nano* **2018**, *12* (7), 6378−6388.

(12) Walther, A.; Timonen, J. V. I.; Díez, I.; Laukkanen, A.; Ikkala, O. Multifunctional High-performance Biofibers Based on Wet-extrusion of Renewable Native Cellulose Nanofibrils. *Adv. Mater.* **2011**, *23* (26), 2924−2928.

(13) Voisin, H.; Bergström, L.; Liu, P.; Mathew, A. P. Nanocellulose-Based Materials for Water Purification. *Nanomaterials* **2017**, *7* (3), No. 57.

(14) Olivetti, E. A.; Cullen, J. M. Toward a Sustainable Materials System. *Science* **2018**, *360* (6396), 1396−1398.

(15) De Gennes, P.-G. Reptation of a Polymer Chain in the Presence of Fixed Obstacles. *J. Chem. Phys.* **1971**, *55* (2), 572−579.

(16) De Gennes, P.-G.; Gennes, P.-G. *Scaling Concepts in Polymer Physics*; Cornell University Press, 1979.

(17) Edwards, S. F. The Statistical Mechanics of Polymerized Material. *Proc. Phys. Soc.* **1967**, *92* (1), No. 9.

(18) Doi, M.; Edwards, S. F. Dynamics of Concentrated Polymer Systems. Part 1.—Brownian Motion in the Equilibrium State. *J. Chem. Soc., Faraday Trans. 2* **1978**, *74*, 1789−1801.

(19) Doi, M.; Edwards, S. F.; Edwards, S. F. *The Theory of Polymer Dynamics*; Oxford University Press, 1988; Vol. *73*.

(20) Perkins, T. T.; Smith, D. E.; Chu, S. Direct Observation of Tube-like Motion of a Single Polymer Chain. *Science* **1994**, *264* (5160), 819−822.

(21) Käs, J.; Strey, H.; Sackmann, E. Direct Imaging of Reptation for Semiflexible Actin Filaments. *Nature* **1994**, *368* (6468), 226−229.

(22) Schleger, P.; Farago, B.; Lartigue, C.; Kollmar, A.; Richter, D. Clear Evidence of Reptation in Polyethylene from Neutron Spin-Echo Spectroscopy. *Phys. Rev. Lett.* **1998**, *81* (1), No. 124.

(23) Richter, D.; Butera, R.; Fetters, L. J.; Huang, J. S.; Farago, B.; Ewen, B. Entanglement Constraints in Polymer Melts. A Neutron Spin Echo Study. *Macromolecules* **1992**, *25* (23), 6156−6164.

(24) Kanematsu, T.; Sato, T.; Imai, Y.; Ute, K.; Kitayama, T. Mutual-and Self-Diffusion Coefficients of a Semiflexible Polymer in Solution. *Polym. J.* **2005**, *37* (2), 65−73.

(25) Nemoto, N.; Makita, Y.; Tsunashima, Y.; Kurata, M. Dynamic Light Scattering Studies of Polymer Solutions. 3. Translational Diffusion and Internal Motion of High Molecular Weight Polystyrenes in Benzene at Infinite Dilution. *Macromolecules* **1984**, *17* (3), 425−430.

(26) Zettl, H.; Häfner, W.; Böker, A.; Schmalz, H.; Lanzendörfer, M.; Müller, A. H. E.; Krausch, G. Fluorescence Correlation Spectroscopy of Single Dye-Labeled Polymers in Organic Solvents. *Macromolecules* **2004**, *37* (5), 1917−1920.

(27) Zettl, U.; Hoffmann, S. T.; Koberling, F.; Krausch, G.; Enderlein, J.; Harnau, L.; Ballauff, M. Self-Diffusion and Cooperative Diffusion in Semidilute Polymer Solutions as Measured by Fluorescence Correlation Spectroscopy. *Macromolecules* **2009**, *42* (24), 9537−9547.

(28) Odijk, T. The Statistics and Dynamics of Confined or Entangled Stiff Polymers. *Macromolecules* **1983**, *16* (8), 1340−1344.

(29) Fakhri, N.; MacKintosh, F. C.; Lounis, B.; Cognet, L.; Pasquali, M. Brownian Motion of Stiff Filaments in a Crowded Environment. *Science* **2010**, *330* (6012), 1804−1807.

(30) Kremer, K.; Grest, G. S. Dynamics of Entangled Linear Polymer Melts: A Molecular-dynamics Simulation. *J. Chem. Phys.* **1990**, *92* (8), 5057−5086.

(31) Skolnick, J.; Kolinski, A.; Yaris, R. Monte Carlo Studies of the Long-Time Dynamics of Dense Polymer Systems. The Failure of the Reptation Model. *Acc. Chem. Res.* **1987**, *20* (9), 350−356.

(32) Fixman, M. Chain Entanglements. I. Theory. *J. Chem. Phys.* **1988**, *89* (6), 3892−3911.

(33) Limbach, H.-J.; Arnold, A.; Mann, B. A.; Holm, C. ESPResSo—an Extensible Simulation Package for Research on Soft Matter Systems. *Comput. Phys. Commun.* **2006**, *174* (9), 704−727.

(34) Usov, I.; Nyström, G.; Adamcik, J.; Handschin, S.; Schütz, C.; Fall, A.; Bergström, L.; Mezzenga, R. Understanding Nanocellulose Chirality and Structure−Properties Relationship at the Single Fibril Level. *Nat. Commun.* **2015**, *6* (1), No. 7564.

(35) Granek, R. From Semi-Flexible Polymers to Membranes: Anomalous Diffusion and Reptation. *J. Phys. II* **1997**, *7* (12), 1761−1788.

(36) Dobrynin, A. V.; Colby, R. H.; Rubinstein, M. Scaling Theory of Polyelectrolyte Solutions. *Macromolecules* **1995**, *28* (6), 1859−1871.

(37) Leibler, L.; Rubinstein, M.; Colby, R. H. Dynamics of Reversible Networks. *Macromolecules* **1991**, *24* (16), 4701−4707.

(38) Hoy, R. S.; Kröger, M. Unified Analytic Expressions for the Entanglement Length, Tube Diameter, and Plateau Modulus of Polymer Melts. *Phys. Rev. Lett.* **2020**, *124* (14), No. 147801.

(39) De Gennes, P. G. Remarks on Entanglements and Rubber Elasticity. *J. Phys. Lett.* **1974**, *35* (9), 133−134.

(40) Kavassalis, T. A.; Noolandi, J. New View of Entanglements in Dense Polymer Systems. *Phys. Rev. Lett.* **1987**, *59* (23), No. 2674.

https://doi.org/10.1021/acs.macromol.3c01526
Macromolecules 2023, 56, 9595−9603

(41) Morse, D. C. Tube Diameter in Tightly Entangled Solutions of Semiflexible Polymers. *Phys. Rev. E* **2001**, *63* (3), No. 31502.
(42) Milner, S. T. Unified Entanglement Scaling for Flexible, Semiflexible, and Stiff Polymer Melts and Solutions. *Macromolecules* **2020**, *53* (4), 1314−1325.
(43) Kröger, M. Shortest Multiple Disconnected Path for the Analysis of Entanglements in Two-and Three-Dimensional Polymeric Systems. *Comput. Phys. Commun.* **2005**, *168* (3), 209−232.
(44) Munk, T.; Höfling, F.; Frey, E.; Franosch, T. Effective Perrin Theory for the Anisotropic Diffusion of a Strongly Hindered Rod. *EPL (Europhys. Lett.)* **2009**, *85* (3), No. 30003.
(45) Ramanathan, S.; Morse, D. C. Simulations of Dynamics and Viscoelasticity in Highly Entangled Solutions of Semiflexible Rods. *Phys. Rev. E* **2007**, *76* (1), No. 10501.
(46) Lang, P.; Frey, E. Disentangling Entanglements in Biopolymer Solutions. *Nat. Commun.* **2018**, *9* (1), No. 494, DOI: 10.1038/s41467-018-02837-5.
(47) Nam, G.; Johner, A.; Lee, N.-K. Reptation of a Semiflexible Polymer through Porous Media. *J. Chem. Phys.* **2010**, *133* (4), No. 044908.
(48) Höfling, F.; Munk, T.; Frey, E.; Franosch, T. Entangled Dynamics of a Stiff Polymer. *Phys. Rev. E* **2008**, *77* (6), No. 60904.
(49) Doi, M. Explanation for the 3.4-power Law for Viscosity of Polymeric Liquids on the Basis of the Tube Model. *J. Polym. Sci., Polym. Phys. Ed.* **1983**, *21* (5), 667−684.
(50) Graessley, W. W.Entangled Linear, Branched and Network Polymer Systems—Molecular Theories. In *Synthesis and Degradation Rheology and Extrusion*; Springer, 1982; Vol. *47*, pp 67−117.
(51) Doi, M.; Graessley, W. W.; Helfand, E.; Pearson, D. S. Dynamics of Polymers in Polydisperse Melts. *Macromolecules* **1987**, *20* (8), 1900−1906.
(52) Marrucci, G. Relaxation by Reptation and Tube Enlargement: A Model for Polydisperse Polymers. *J. Polym. Sci., Polym. Phys. Ed.* **1985**, *23* (1), 159−177.
(53) Read, D. J.; Jagannathan, K.; Likhtman, A. E. Entangled Polymers: Constraint Release, Mean Paths, and Tube Bending Energy. *Macromolecules* **2008**, *41* (18), 6843−6853.
(54) Rubinstein, M.; Colby, R. H. Self-consistent Theory of Polydisperse Entangled Polymers: Linear Viscoelasticity of Binary Blends. *J. Chem. Phys.* **1988**, *89* (8), 5291−5306.
(55) Fixman, M. Entanglements of Semidilute Polymer Rods. *Phys. Rev. Lett.* **1985**, *54* (4), No. 337.
(56) Fixman, M. Dynamics of Semidilute Polymer Rods: An Alternative to Cages. *Phys. Rev. Lett.* **1985**, *55* (22), No. 2429.
(57) Bitsanis, I.; Davis, H. T.; Tirrell, M. Brownian Dynamics of Nondilute Solutions of Rodlike Polymers. 1. Low Concentrations. *Macromolecules* **1988**, *21* (9), 2824−2835.
(58) Bitsanis, I.; Davis, H. T.; Tirrell, M. Brownian Dynamics of Nondilute Solutions of Rodlike Polymers. 2. High Concentrations. *Macromolecules* **1990**, *23* (4), 1157−1165.
(59) Córdoba, A.; Schieber, J. D. MUnCH: A Calculator for Propagating Statistical and Other Sources of Error in Passive Microrheology. *Rheol. Acta* **2022**, *61* (1), 49−57.
(60) Xu, J.; Palmer, A.; Wirtz, D. Rheology and Microrheology of Semiflexible Polymer Solutions: Actin Filament Networks. *Macromolecules* **1998**, *31* (19), 6486−6492.
(61) Naderi, A.; Lindström, T.; Pettersson, T. The State of Carboxymethylated Nanofibrils after Homogenization-Aided Dilution from Concentrated Suspensions: A Rheological Perspective. *Cellulose* **2014**, *21* (4), 2357−2368.
(62) Geng, L.; Mittal, N.; Zhan, C.; Ansari, F.; Sharma, P. R.; Peng, X.; Hsiao, B. S.; Söderberg, L. D. Understanding the Mechanistic Behavior of Highly Charged Cellulose Nanofibers in Aqueous Systems. *Macromolecules* **2018**, *51* (4), 1498−1506.
(63) Nordenström, M.; Benselfelt, T.; Hollertz, R.; Wennmalm, S.; Larsson, P. A.; Mehandzhiyski, A.; Rolland, N.; Zozoulenko, I.; Söderberg, D.; Wågberg, L. The Structure of Cellulose Nanofibril Networks at Low Concentrations and Their Stabilizing Action on Colloidal Particles. *Carbohydr. Polym.* **2022**, *297*, No. 120046.

https://doi.org/10.1021/acs.macromol.3c01526
Macromolecules 2023, 56, 9595−9603